

**Teresa Mineo · George W. Fraser ·
Adrian Martindale · Charly Feldman ·
Riccardo Campana · Giancarlo
Cusumano · Marco Feroci**

Abstract The Large Observatory For X-ray Timing (LOFT) is one of the candidate missions selected by the European Space Agency for an initial assessment phase in the Cosmic Vision programme. It is proposed for the M3 launch slot and has broad scientific goals related to fast timing of astrophysical X-ray sources. LOFT will carry the Large Area Detector (LAD), as one of the two core science instruments, necessary to achieve the challenging objectives of the project. LAD is a collimated detector working in the energy range 2-50 keV with an effective area of approximately 10 m^2 at 8 keV.

On behalf of LOFT collaboration

G.W. Fraser, A. Martindale, C. Feldman
Space Research Centre, Michael Atiyah Building, Department of Physics and Astronomy,
University of Leicester, LE1 7RH, Leicester, UK

ity is derived from a limited set of laboratory measurements, used to constrain the model. The measurements were taken using a prototype collimator whose thickness is similar to that adopted in the current baseline design proposed for the LAD.

We find that the experimentally measured level of reflectivity of the pore inner walls enhances the off-axis transmission at low energies, producing an almost flat-top response. The resulting background increase due to the diffuse cosmic X-ray emission and sources within the field of view does not degrade the instrument sensitivity.

Keywords X-ray optics, X-ray collimator, microchannel plate, capillary reflection, LOFT

PACS 07.85.Fv · 07.87.+v · 95.55.Ka

1 Introduction

LOFT [5] is devoted to study matter in extreme states such as those found at the event horizon of black holes or the surface of neutron stars. These sources exhibit rapid luminosity changes and spectral variability in the X-ray region, providing the key scientific justification for the Large Area Detector [LAD; 21] one of the two core scientific instruments proposed for LOFT.

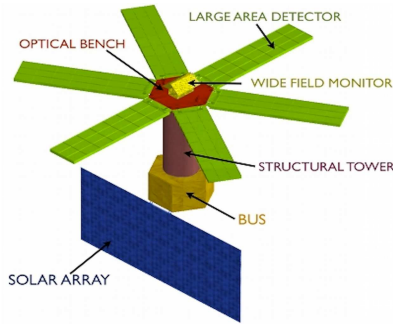


Fig. 1: Baseline configuration for the LOFT satellite; the six green panels together form the LAD.

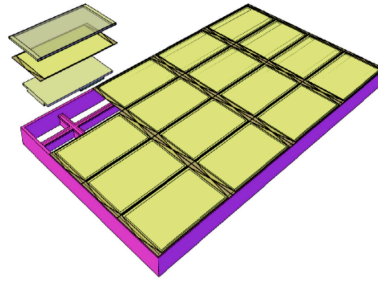


Fig. 2: Schematic of the LAD Module, the exploded section shows (from top down) the mounting of the collimator, SDD and the Front End Electronics board.

The LAD is a collimated detector based on Silicon Drift Detectors (SDD) that work in the energy range 2-50 keV with an effective area of approximately 10 m^2 at 8 keV, an energy resolution of 4% at 6 keV and a timing accuracy of $10 \mu\text{s}$.

The LAD detector consists of 2016 SDDs located in six deployable panels (see

Fig. 1) and organized as shown in Fig. 2 in modules of 16 elements mechanically and electrically linked to form a single coherent instrument. The SDD version adopted for LAD is an optimization of the model used in ALICE, an experiment of the Large Hadron Collider at CERN [17; 14; 1].

The Field of View (FoV) is limited by a collimator placed in front of the detector, in order to reduce the background contamination from off-axis point sources and the diffuse cosmic X-ray background (CXB). Its design requires a trade-off as introducing a collimator drastically reduces background from off-axis sources, but produces a varying instrument response with off-axis angle. Hence, care is required to avoid spurious modulations in the detected signals caused by the limitations of the precision of spacecraft attitude control and by pointing stability ($\sim 1'$ for the LAD).

Following the heritage of the EXOSAT instruments MEDA [16] and GSPC [13] and, more recently, the collimator on the BepiColombo Mercury Imaging X-ray Spectrometer [MIXS-C; 6], the technology adopted for the LAD is based on lead-glass microchannel plates (MCP). This type of collimator provides a transmission function that is suitable for the scientific objectives of LOFT mission, while minimizing the mass per unit area - as required by the large surface area that must be covered for LOFT (active area $\sim 15 \text{ m}^2$).

An effect of primary importance for LAD performances is that X-ray photons with small grazing incident angles (lower than a few degrees) can be reflected by the inner walls of the pores in lead glass collimators according to the total reflection theory [19; 7; 10]. This effect increases the collimator transmission at off-axis angles, rounding or flattening the transmission profile, but also enhancing the background contribution from CXB and field sources - degrading instrument sensitivity.

In this paper, we present an ad-hoc study to evaluate the influence of channel reflectivity on the instrument performance. Section 2 presents details of the collimator chosen in the LAD baseline design. Section 3 presents a limited experimental measurement of a prototype collimator, used to constrain the reflectivity model reported in Section 4. Section 5 presents the results of a simulator for the instrument's response (including the transmission function of the collimator and the level of detected CXB) and Section 6 describes the conclusions of our study.

2 The collimator

The collimator adopted for the LAD is summarized in Table 1 and comprises an array of 8×11 cm MCPs which are held ~ 2 mm above the SDD input face by a Titanium frame. Sixteen SDDs and collimators are held in an Al detector housing which constitutes a module (Fig. 2).

MCPs are made by a draw and etch process similar to how optical fibres are produced [12]. A lead-glass core, is surrounded by a cladding glass, forming a couple which is drawn and stacked to produce a multi-fibre. These are then stacked and fused to produce a block, which which can be sliced, polished

to the required thickness and etched to produce the finished plates. The wall of the pores are therefore made of the cladding glass, with a density of 3.3 gm cm^{-3} and Pb fraction ($\sim 37\%$ by weight) guaranteeing good absorption of X-rays in the pore septa in the 2-30 keV energy band of LAD.

This configuration gives an open area ratio of $\sim 70\%$, an aspect ratio of 60:1 and a geometrical FoV of $\sim 1^\circ$. The transmission function presents a moderate dependence on the azimuthal angle ϕ (relative to the axes defined by the Cartesian pore walls) because of the square shape of the pore. In particular, moving from $\phi=0^\circ$ to $\phi=45^\circ$, the geometrical collimator transmission is reduced by $\sim 4\%$ at $5'$ and by $\sim 15\%$ at $15'$.

A blanket of 80 nm Al supported by $1 \mu\text{m}$ Kapton, placed either above or below the MCPs, shields LAD against UV, optical, and infrared light contamination. Moreover a second Al film, 80 nm thick, is deposited on top to thermally insulate the collimator and provide a second layer of light rejection. This second layer offers added resilience against light ingress through pinholes in the foils.

The collimator transmission function is influenced by misalignments coming from a number of sources as mounting tolerances between the optical axis and the deployable panels, or between the separate collimators or modules. The pore-to-pore alignment in the MCP itself is not negligible. Moreover, time variable effects exist, such as those induced by thermal deformations of panels and modules during the different thermal loading around an orbit. To maintain LAD performances within the requirements derived from the proposed scientific objectives, the total misalignment error budget must be of order $2.5'$ where the contribution from pore orthogonality is $\sim 1'$.

The polishing of the couple prior to drawing and the drawing process itself lead to pore surfaces that are intrinsically smooth. Subsequent removal of the core glass by acid etch [18; 20] produces a silicon-rich layer in the inner surface of the pores where lead and other elements have been leached out [4]. Moreover, a roughening of the inner pore surface may occur, whose level depends on several factors, including the etching uniformity, irregularity of the core glass surface or diffusion effects across the glass boundaries [10]. These combined effects lead to the reflectivity of the channel pore wall and must be accounted for in the theoretical model described below.

3 Laboratory measurements

We have evaluated the capillary reflectivity of a representative sample collimator which was 5mm in thickness - similar to the final design value for the LAD collimator. This sample has a 250:1 aspect ratio, $20 \mu\text{m}$ pore width and $6 \mu\text{m}$ septal thickness. No Al film is deposited on its input surface (as called for in the LAD design), however, this should have no influence on the comparison to the Monte Carlo model which is of primary importance here. An electron microscope image of the sample is shown in Fig. 3.

Table 1: Characteristics of the LAD collimator

Parameter	Value
pore size	100.0 μm
septal thickness	20.0 μm
collimator thickness	6.0 mm
open area fraction	70%
aspect ratio	60:1
Al film thickness	80.0 nm
blanket Kapton thickness	1.0 μm
blanket Al thickness	80.0 nm
collimator-focal plane distance	2.0 mm
total misalignment error budget	2.5'

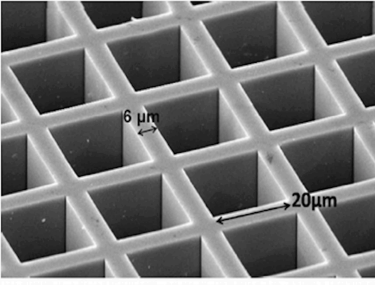


Fig. 3: Electron microscope image of the collimator used in the laboratory measurements for evaluating pore reflectivity.

Table 2: Relative transmission at 2.4 KeV from laboratory measurements

Angle (arcmin)	Transmission
0	1.00 ± 0.020
5	0.89 ± 0.018
10	0.82 ± 0.017
15	0.66 ± 0.015
20	0.42 ± 0.011
25	0.17 ± 0.006
30	0.07 ± 0.004
35	0.03 ± 0.002

The measurements were performed in the University of Leicester's 28m long beamline. At the X-ray source end, an electron bombardment source with a Molybdenum anode was used to stimulate the Mo-L fluorescence lines with an average energy of ~ 2.4 keV. An accelerating potential of 4keV and a 1 μm Ag filter were used to isolate the region of the emission lines and maximise the line to continuum ratio.

The collimator was held in a two axis rotation stage, a distance of 27 m from the X-ray source in order to minimise the effect of beam divergence. A large area MCP detector [11] was placed behind the collimator to measure changes in the intensity of the radiation passing through the collimator as a function of off-axis angle. The measurements were performed by rotating the collimator incrementally by steps of 5'. The ratio between the detector count rate at each angle and the on-axis value are shown in Table 2.

The errors in the count rate are dominated by the dark noise of the detector, where radioactive isotopes in the detector glass lead to a non-zero background. The errors reported in the table reflect this, of paramount importance here is

the ratio of the input count rate and the detector noise over the relevant area of the detector. Although the source generates a large emission rate for X-rays, the solid angle subtended by the collimator at 27 m is small, making it difficult to improve the signal to noise significantly without compromising on beam divergence.

4 The code

The experimentally obtained transmission function includes several effects which cannot be deconvolved easily during data analysis, including: beam divergence, MCP pore misalignment and pore wall reflectivity. A ray-tracing simulator allows a mathematical approach to deducing the major contributors to the transmission function, by computing a transmission function for comparison with the empirical data.

The simulator is a stand-alone ray-tracing code which models the interactions of X-ray photons with the collimator and follows them to the detector surface. The photon interaction processes, in all stages, are governed by Montecarlo calculations. The flow chart of the code is presented in Fig. 4.

The collimator is defined as a solid parallelogram with a porous structure, where each pore is described as an empty parallelogram identified by the coordinates of its centre and by the width of the sides. Both filters are simulated directly in front of the collimator. MCP pore misalignments are taken into account by varying the photon incident direction by an angle randomized from a Gaussian distribution whose standard deviation is given as an input parameter.

Source photons can either be simulated with monochromatic energy or drawn from spectral distributions introduced as tables, the nature of the source can be either point-like or diffuse and it may be located at either finite or infinite distance from the collimator. The modelled detection surface has the same geometrical area as the collimator and no detector response is included.

Each photon is characterised by a direction, an energy and an impact position randomly distributed on the collimator surface. If not absorbed by the filters, photons can be either directly transmitted to the focal plane or interact with the collimator. In the latter case, they can either be absorbed by the structure or interact with the pore wall: multiple interactions within a pore can happen before the photon is absorbed or reach the detection surface. If a photon is reflected, its output direction is computed from Snell law.

The filter transmission depends on energy and incident angle and is computed evaluating the thickness crossed by the photon and interpolating the cross-sections of the involved materials from tables retrieved from the National Institute of Standards and Technology (NIST) database¹. Figure 5 shows the total transmission probability of the blanket and the Al filter as function of energy: we note that they produce a reduction of $\sim 15\%$ at 2 keV and $< 1\%$ at 6 keV in the collimator effective area.

¹ <http://www.nist.gov/index.html>

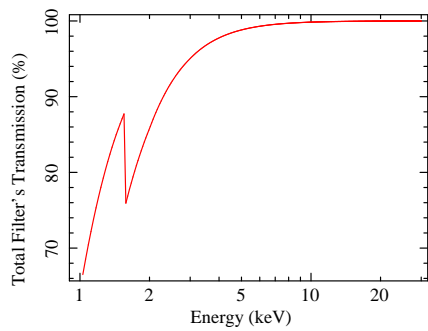
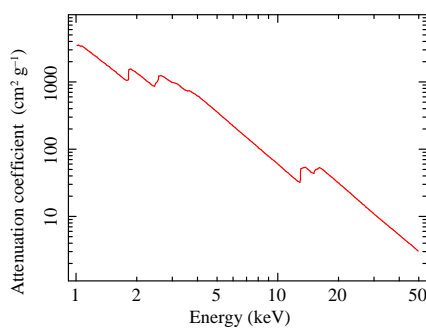


Fig. 5: Total transmission efficiency of the two filters applied to the collimator.



elements are leached during the etching process [4], we used reflectivity tables for SiO₂ in the simulations presented in this paper.

The analysis methodology applied in our work assumes that the level of micro-roughness is sufficient to characterize the reflectivity i.e. micro-roughness is dominant. This hypothesis is based on the observation that the fraction of photons that reach the focal plane after reflection is lower than 20% at any incident angle. Moreover, only 2% of these scattered photons experience multiple scatterings.

We computed the transmission function at each value of micro-roughness and compared it to the empirical data, choosing the best fit as the one that minimises the root mean square (*rms*) of the differences between the measured and the simulated data. We adopted this as our reflectivity model in the calculations that follow. In these simulations, we assumed $1'$ as level of misalignments in the pore orthogonality [10].

We found that data are best reproduced by the reflectivity profile from 14 nm surface micro-roughness. This level of micro-roughness is, quite significantly higher than values quoted in literature for lead glass MCPs [10; 8] and is probably due to the very large aspect ratio of the channels in this collimator. The reflection probability is shown in Fig. 7, for an incident angle of 10° , as function of energy and in Fig. 8 as function of the off-axis angle for 2 keV and 6 keV photons.

The top panel of Fig. 9 presents a comparison between the relative transmission obtained by the simulator (red line) assuming 14 nm micro-roughness and the data derived from laboratory measurements (black circles) as function of the off-axis angles. The percentage differences between the measured and the simulated data relative to the measured values is displayed in the bottom panel of the same figure. The discrepancy is lower than 30% for all angles and lower than 10% up to 20'.

For comparison, in the top panel Fig. 9 the transmission function obtained fixing the micro-roughness level to 10 nm (green line) and 18 nm (grey line)

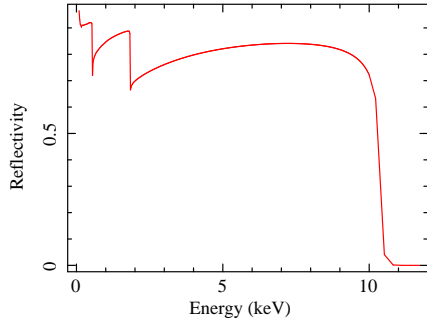


Fig. 7: Glass reflectivity relative to a surface micro-roughness of 14 nm vs energy for an incident angle of 10° .

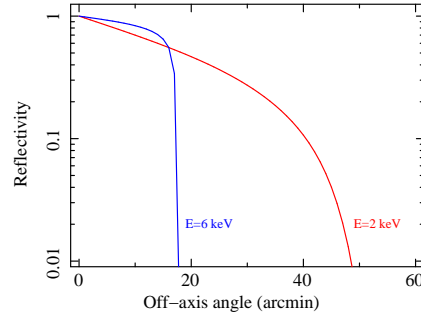


Fig. 8: Glass reflectivity relative to a surface micro-roughness of 14 nm vs off-axis angles for 2 keV (red curve) and 6 keV (blue curve).

together with the triangular response expected for a 250:1 aspect ratio collimator (blue line) are also shown.

5 Simulator Results

Both the capillary reflectivity described above and the intrinsic misalignments in the collimator axes (both due to the MCP collimator itself and errors introduced by assembly and alignment tolerances of the modules and panels) affect the LAD sensitivity by altering the transmission function. These errors lead to reduced effective area for on-axis sources and increased background from off-axis point sources and the diffuse X-ray background reducing the overall sensitivity. These effects are quantified here by including the reflectivity model constrained by lab data in the LAD simulator and by assuming a total misalignment error of $2.5'$ (the total error budget). In practice, this is all attributed to pore orthogonality in the simulator, however, this simplification will have no impact on the results.

5.1 Transmission function

The collimator transmission function is modified by the capillary reflectivity and by misalignments. The misalignments introduce a reduction of the effective area on-axis and increase the amount of background collected from off-axis, this effect is almost independent of energy and mainly confined to small incident angles determined by the overall alignment errors. The effect of reflectivity is more subtle. For a perfect collimator with no alignment errors, it has no effect on-axis as no area of channel walls are projected towards the source, however, it does allow increased collection of background from off-axis.

For a real collimator, with intrinsic misalignments, the effect is more complex - for on-axis sources the reflectivity allows rays to continue to reach the detector plane even though they have hit a wall, meaning the effect of misalignments is decreased. However, it is generally true that significant reflectivity will reduce sensitivity as more background will be collected.

For the values adopted in the simulations, the largest reduction in effective area due to misalignments ($\sim 5\%$) is completely cancelled in the energy range 2 –17 keV by the reflectivity enhancement. This is shown in Fig. 10 where the ratio between the transmission with and without reflectivity is plotted as function of energy for two incident angles.

The transmission function including reflectivity and misalignment effects is shown in Fig. 11 for a source at infinite distance with monochromatic X-rays of 3 keV (red curve) and 6 keV (green curve). For comparison, the canonical triangular shape is also shown with a blue curve. We note that in both curves the reduction of the transmission function with respect to the on axis value is lower than for the triangular one at small angles ($< 10'$). In particular, the decrease of the effective area is less than 5% up to $10'$ for 3 keV photons.

Considering that X-ray spectra decrease with energy, we evaluated the reduction expected in the observed rate of a typical source located $5'$ off-axis whose spectrum is modelled by a power law with photon index $\alpha=2$. We found that the rate is lowered by $\sim 1\%$ with respect to the on axis value, and comparing this to the reduction expected from a pure geometrical collimator ($\sim 8\%$), the adopted level of reflectivity produces a flat response within the alignment accuracy angles (at least at 6keV), meaning that spurious modulations due to pointing accuracy are minimised.

5.2 Diffuse Background

A drawback of this flatter transmission function is the increase of the diffuse background that reaches the focal plane with a consequent degradation in sensitivity. We evaluated the effect of the capillary reflectivity on the level of the transmitted CXB simulating a uniformly distributed diffuse source with photon directions randomizes up to an off-axis angle of $70'$ and energies E drawn in the range 2–30 keV according to the model [9]:

$$\Phi(E) = 7.877 E^{-1.29} \exp(-E/41.13) \quad \text{photons cm}^{-2}\text{s}^{-1}\text{sr}^{-1}\text{keV}^{-1} \quad (1)$$

The CXB rate at the focal plane is obtained by convolving the spectrum transmitted by the collimator with the detector response matrix: the result is shown in Fig. 12 (red line). This result agrees (within the statistical errors) with the spectrum published in Campana et al. (2013) obtained using the reflectivity of lead-glass.

Comparing the spectrum with the one obtained without pore wall reflectivity and misalignments, the highest increase is observed below 4 keV where an increase of $\sim 35\%$ is detected. At higher energies, the reflectivity contribution

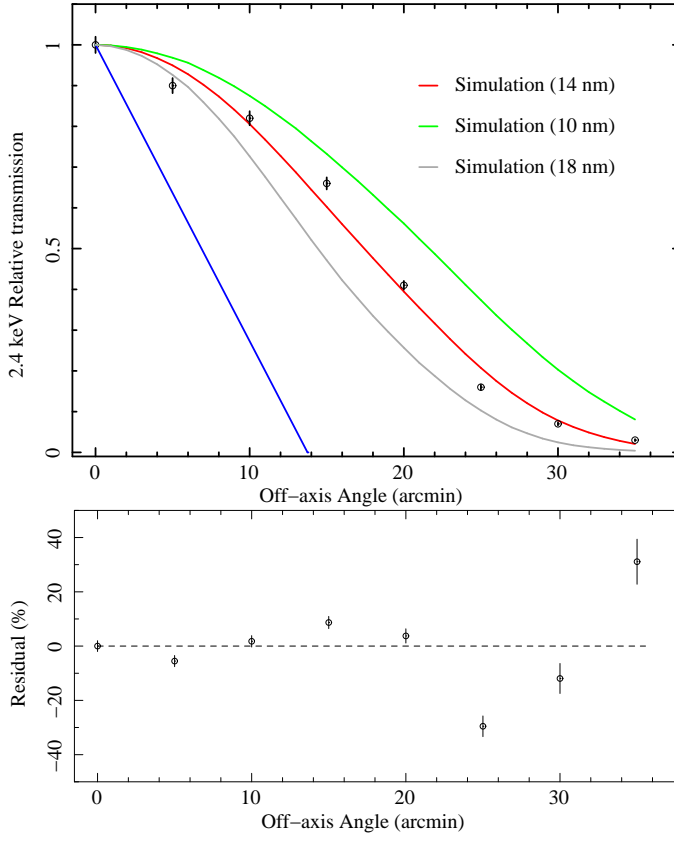


Fig. 9: *Top Panel:* The red curve shows the transmission function obtained with the simulator fixing the micro-roughness level to 14 nm vs the off-axis angles. Lab data are indicated with black points. The green and grey curves represent the transmission function obtained fixing the micro-roughness level to 10 nm and 18 nm, respectively. The triangular response expected for a 250:1 aspect ratio collimator is also shown with the blue line. *Bottom Panel:* Differences in percentage between the measured and the simulated values normalized to the measured ones vs the off-axis angle.

reduces and the CXB increase is $\sim 20\%$ in the range 4–6 keV and only $\sim 10\%$ in the range 6–10 keV.

5.3 Discussion of the results

We found that reflectivity induces a significant increase of the transmission function at low angles. Consequently, the CXB background is increased dependant on the energy and direction of the incident photon.

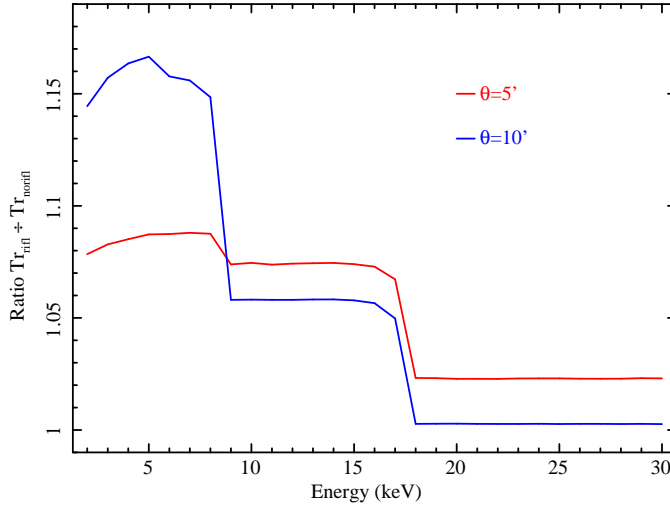


Fig. 10: Increasing factor of the collimator transmission due to the capillary reflection vs energy for a parallel beam at 5' (red curve) and 10' (blue curve) off-axis angles.

LOFT's scientific objectives require the observations of sources up to fluxes of 1-10 mCrab ($10^{-11} - 10^{-12} \text{ erg cm}^{-2} \text{ s}^{-1}$). This can be achieved if the level of background is kept lower than 10 mCrab (equivalent to $1.6 \times 10^{-2} \text{ counts cm}^{-2} \text{ s}^{-1}$) in the nominal 2-30 keV energy range. From a detailed study,

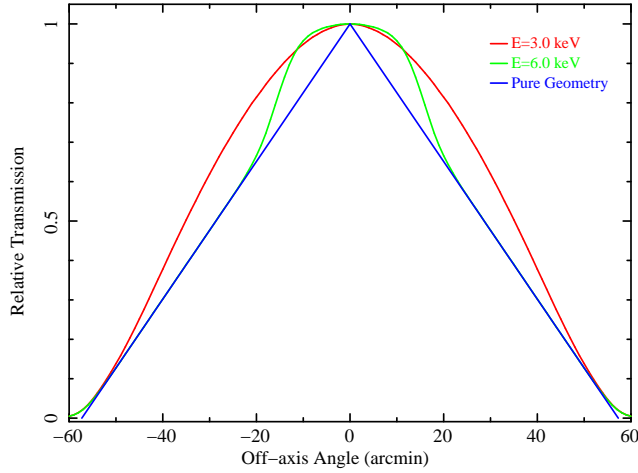


Fig. 11: Transmission function vs off-axis angles: the red curve is relative to the energy of 3 keV; the green curve to the energy 6 keV. For comparison, the canonical transmission curve obtained without reflection is shown in blue.

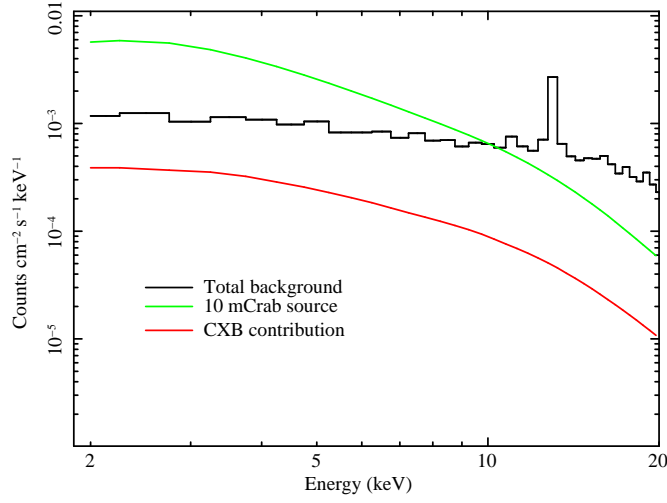


Fig. 12: The red line indicates the simulated spectrum of the CXB observed by the LAD. The black line is the total background obtained by [2]. For comparison, the spectrum of a 10 mCrab source is shown with the green line.

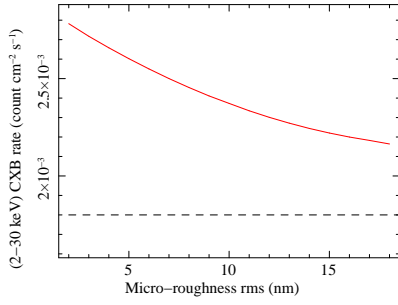


Fig. 13: Rate of the CXB at the focal plane vs the *rms* of the surface micro-roughness. The dashed line indicates the rate obtained without capillary reflectivity.

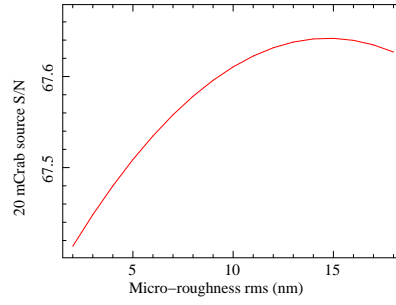


Fig. 14: Signal to Noise ratio for a 20 mCrab source vs the *rms* of the surface micro-roughness.

performed with a Geant4 simulator, the background rate at the satellite orbit from all expected components, except CXB, is 1.2×10^{-2} counts $\text{cm}^{-2} \text{s}^{-1}$ [2]. The rate of the diffuse cosmic X-ray background obtained with our simulations is 2.2×10^{-3} counts $\text{cm}^{-2} \text{s}^{-1}$, hence, the measured level of micro-roughness produces a CXB level compatible with the requirements. The total background and the spectrum of a 10 mCrab source (assuming the Crab spectrum) are shown in Fig. 12 with a black and a green line, respectively.

The larger transmission function at low energies could also worsen the contamination from off-axis sources making the observation of crowded fields such as the Galactic bulge and plane difficult because of source confusion. To evaluate this effect, we used the Swift BAT 54 month catalogue [3] that includes 1256 sources and selected 65 sources whose flux is $>10\text{mCrab}$ in the energy range 15-150 keV. Assuming a power law spectrum with photon index $\alpha=2$ (Crab-like), we computed the LAD rate of these sources in the range 2-30 keV and the contamination from all sources within an angular distance of 1° . The number of sources whose spectrum will be contaminated for more than 10% is statistically equivalent to the number obtained with the triangular transmission function.

We can conclude that the reflectivity measured in the lab collimator does not degrade the required LAD performances.

In order to determine what impact different micro-roughness would have on signal to noise in the LAD band Fig 13 and Fig. 14 show the calculated level of CXB background and the detection significance of a Crab-like source (with a flux of 20mCrab) at values of micro-roughness close to the measured one. We observe that the CXB rate has a maximum variation of 20% in the investigated range and its value at 14 nm micro-roughness is only $\sim 30\%$ higher than the one obtained without capillary reflectivity, shown in Fig 13 with a dashed line. However, because the statistical significance of a typical 20mCrab source improves with *rms*, values of micro-roughness lower than 10 nm are not recommended.

6 Summary and conclusion

We obtained a model of the reflectivity from the inner walls of the pores in the LAD collimator and verified them against a set of empirical measurements. Lab data were best fit assuming reflectivity from SiO_2 with a surface micro-roughness of 14 nm; it is believed that the extreme channel lengths explain the difference between this and prior lower published values for the surface micro-roughness.

Including these results in the simulator and taking into account the total misalignments assumed for the LAD, we compute the transmission function and, hence, the level of CXB at the focal plane in order to evaluate the effects of reflectivity on the collimator performance.

We conclude that capillary reflectivity with a level of micro-roughness close to that measured experimentally does not degrade the collimator performance significantly.

Acknowledgements Authors acknowledge the financial support from the Italian INAF Tecno-PRIN 2009 and ASI/INAF contract I/021/12/0, and from the UK Space Agency.

References

1. Beolè, S., Alessandro, B., Antinori, S., Coli, S., Costa, F., Crescio, E., Falchieri, D., Arteché Diaz, R., Di Liberto, S., Giraudo, G., Giubellino, P., Masetti, G., Mazza, G., Meddi, F., Prino, F., Rashevsky, A., Riccati, L., Rivetti, A., Senyukov, S., Simonetti, L., Toscano, L., Tosello, F., Urciuoli, G. M., Vacchi, A., Wheadon, R., The ALICE silicon drift detectors: Production and assembly, *Nuclear Instruments and Methods in Physics Research A*, 582, 733, (2007)
2. Campana, R., Feroci, M., Del Monte, E., Mineo, T., Lund, N., Fraser, G.W., Background simulations for the Large Area Detector Experimental Astronomy, 29, (2013)
3. Cusumano, G., La Parola, V., Segreto, A., Ferrigno, C., Maselli, A., Sbaruffatti, B., Romano, P., Chincarini, G., Giommi, P., Masetti, N., Moretti, A., Parisi, P., Tagliaferri, G. The Palermo Swift-BAT hard X-ray catalogue. III. Results after 54 months of sky survey *Astronomy and Astrophysics*, 24, 64, (2010)
4. D'Souza, A., Pantano, C.G. Surface layer formation due to leaching and heat treatment of alkali lead silicate glass *Physics and chemistry of glasses*, 37, 79, (1996)
5. Feroci, M., Stella, L., Vacchi, A., Labanti, C., Rapisarda, M., Attina, P., Belloni, T., Campana, R., Campana, S., Costa, E., Del Monte, E., Donnarumma, I., Evangelista, Y., Israel, G. L., Muleri, F., Porta, P., Rashevsky, A., Zampa, G., Zampa, N., Baldazzi, G., Bertuccio, G., Bonvicini, V., Bozzo, E., Burderi, L., Corongiu, A., Covino, S., Dall'Osso, S., de Martino, D., di Cosimo, S., di Persio, G., di Salvo, T., Fuschino, F., Grassi, M., Lazzarotto, F., Malcovati, P., Marisaldi, M., Mastropietro, M., Mereghetti, S., Morelli, E., Orio, M., Pellizzoni, A., Pacciani, L., Papitto, A., Piccoli, L., Possenti, A., Rubini, A., Soffitta, P., Turolla, R., Zampieri, L., LOFT: a large observatory for x-ray timing, *Proceedings of the SPIE*, 7732, 1, (2010)
6. Fraser, G. W., Carpenter, J. D., Rothery, D. A., Pearson, J. F., Martindale, A., Huvelin, J., Treis, J., Anand, M., Anttila, M., Ashcroft, M., Benkoff, J., Bland, P., Bowyer, A., Bradley, A., Bridges, J., Brown, C., Bulloch, C., Bunce, E. J., Christensen, U., Evans, M., Fairbend, R., Feasey, M., Gianini, F., Hermann, S., Hesse, M., Hilchenbach, M., Jorden, T., Joy, K., Kaipainen, M., Kitchingman, I., Lechner, P., Lutz, G., Malkki, A., Muinonen, K., Näränen, J., Portin, P., Prydderch, M., Juan, J. S., Sclater, E., Schyns, E., Stevenson, T. J., Strüder, L., Syrjasuo, M., Talboys, D., Thomas, P., Whitford, C., Whitehead, S., The mercury imaging X-ray spectrometer (MIXCS) on *bepicolombo*, *Planetary and Space Science*, 58, 79, (2010)
7. Fraser, G. W., Brunton, A. N., Lees, J. E., Pearson, J. F., Willingale, R., Emberson, D. L., Feller, W. B., Stedman, M., Haycocks, J., Development of microchannel plate (MCP) x-ray optics, *Proceedings of the SPIE*, 2011, 215, (2011)
8. Fraser, G. W. , Lees, J. E. , Pearson, J. F. , Sims, M. R., Roxburgh, K., X-ray focusing using microchannel plates, *Society of Photo-Optical Instru-*

- mentation Engineers (SPIE) Conference Series, 1546, 41, (1992)
9. Gruber, D. E., Matteson, J. L., Peterson, L. E., Jung, G. V., The Spectrum of Diffuse Cosmic Hard X-Rays Measured with HEAO 1, *Astrophysical Journal*, 520, 124, (1999)
10. Kaaret, P., Geissbuehler, P., Chen, A., Glavinas, E., X-ray focusing using microchannel plates, *Applied Optics* (ISSN 0003-6935), 31, 7339, (1992)
11. Lees, J. E. and Pearson, J. F., A large area MCP detector for X-ray imaging, *Nuclear Instruments and Methods in Physics Research A*, 384, 410, (1997)
12. Martin, A.P., X-ray optics, University of Leicester, PhD thesis, (2000)
13. Peacock, A., Andresen, R. D., Manzo, G., Taylor, B. G., Villa, G., Re, S., Ives, J. C., Kellock, S. The gas scintillation proportional counter on EXOSAT, *Space Science Reviews*, 30, 525, (1981)
14. Rashevsky, A., Bonvicini, V., Burger, P., Piano, S., Piemonte, C., Vacchi, A., Large area silicon drift detector for the ALICE experiment, *Nuclear Instruments and Methods in Physics Research A*, 485, 54, (2002)
15. Revnivtsev, M., Molkov, S., Sazonov, S., Large-scale variations of the cosmic X-ray background and the X-ray emissivity of the local Universe, *Astronomy and Astrophysics*, 483, 425, (2008)
16. Turner, M. J. L., Smith, A., Zimmermann, H. U., The medium energy instrument on EXOSAT, *Space Science Reviews*, 30, 513, (1981)
17. Vacchi, A., Castoldi, A., Chinnici, S., Gatti, E., Longoni, A., Palma, F., Sampietro, M., Rehak, P., Kemmer, J., Performance of the UA6 large-area silicon drift chamber prototype, *Nuclear Instruments and Methods in Physics Research A*, 306, 187, (1991)
18. Wallace, K., Collon, M., Bavdaz, M., Fairbend, R., Séguy, J., Krumrey, M., Developments in glass micro pore optics for x-ray applications, *Proceedings of the SPIE*, 6266, 62661A, (2006)
19. Willingale, R., Fraser, G. W., Brunton, A. N., Martin, A. P., Hard X-ray imaging with microchannel plate optics”, *Experimental Astronomy*, 8, 281, (1998)
20. Wiza, J. L., Microchannel plate detectors *Nuclear Instruments and Methods*, 162, 587, (1979)
21. Zane, S., Walton, D., Kennedy, T., Feroci, M., Den Herder, J.-W., Ahangarianabhari, M., Argan, A., Azzarello, P., Baldazzi, G., Barret, D., Bertuccio, G., Bodin, P., Bozzo, E., Cadoux, F., Cais, P., Campana, R., Coker, J., Cros, A., Del Monte, E., De Rosa, Alessandra, Di Cosimo, S., Donnarumma, I., Evangelista, Y., Favre, Y., Feldman, C., Fraser, G., Fuschino, F., Grassi, M., Hailey, M. R., Hudec, R., Labanti, C., Macera, D., Malcovati, P., Marisaldi, M., Martindale, A., Mineo, T., Muleri, F., Nowak, M., Orlandini, M., Pacciani, L., Perinati, E., Petracek, V., Pohl, M., Rachevski, A., Smith, P., Santangelo, A., Seyler, J.-Y., Schmid, C., Soffitta, P., Suchy, S., Tenzer, C., Uttley, P., Vacchi, A., Zampa, G., Zampa, N., Wilms, J., Winter, B., A large area detector proposed for the Large Observatory for X-ray Timing (LOFT), *Proceedings of the SPIE*, 8443, 2, (2012)